ELSEVIER

Physica C 249 (1995) 339–349

PHYSICA C

Study of flux behavior in $Bi_2Sr_2CaCu_2O_8$ single crystal in external magnetic fields up to 1 T

M.R. Koblischka [a,*,1], R.J. Wijngaarden [a], D.G. de Groot [a], R. Griessen [a], A.A. Menovsky [b], T.W. Li [c]

[a] *Vrije Universiteit, Faculteit der Natuurkunde en Sterrenkunde, De Boelelaan 1081, 1081 HV Amsterdam, The Netherlands*
[b] *Van der Waals–Zeeman Laboratory, University of Amsterdam, Valckenierstraat 65, 1018 XE Amsterdam, The Netherlands*
[c] *Kamerlingh Onnes Laboratorium, Rijksuniversiteit Leiden, PO. Box 9506, 2300 RA Leiden, The Netherlands*

Received 21 March 1995

Abstract

Using the high-resolution Faraday effect (HRF) technique, the behavior of magnetic flux in $Bi_2Sr_2CaCu_2O_8$ single crystals is visualized in external magnetic fields up to 1 T. This technique reveals defects in many of these crystals which are probably twin planes. X-ray measurements indicate that two adjacent crystallites have *c*-axis lattice vectors which deviate from each other by about one degree. As a consequence of these defects, the shielding currents break up in sub-loops, each shielding a defect-free part of the sample. This leads to an underestimate of the critical current values determined by non-local magnetization measurements. Magneto-optical images can be used to calculate the necessary correction.

1. Introduction

Most of the magnetic measurements on high-T_c superconductors are of the integral type, i.e. they are sensitive only to the total magnetic moment of a sample. This is the case for various kinds of magnetometers and AC susceptibility techniques. A major disadvantage of these techniques is that they are completely insensitive to the current and flux *distributions* in the superconductor. On the other hand, the magneto-optical visualization of flux in a superconductor is a powerful tool to study directly the interaction of defects in the sample with the flux lines [1]. From such observations, one can determine many important characteristics locally such as the pinning force and current density [2–7]. We have used the high-resolution Faraday effect (HRF) technique both to observe the flux penetration with a relatively high spatial resolution (≈ 0.5 μm) [8] and to study the time evolution of the flux patterns in an external magnetic field [9,10]. Studies of this kind were performed up to now mostly in the $YBa_2Cu_3O_{7-\delta}$ system on single crystals, thin films and polycrystalline samples [9,11,12]. On $Bi_2Sr_2CaCu_2O_{8-\delta}$ (Bi-2212) similar investigations are lacking in the literature although it is a most interesting compound

* Corresponding author.
[1] Present address: Université de Genève, Groupe de Physique appliquée, rue d'Ecole de Medecine 20, CH-1211 Genève 4, Switzerland.

SSDI 0921-4534(95)00323-1

because of its large anisotropy [14,15]. Only the pinning effect of columnar defects created by heavy-ion irradiation was carefully studied [13].

In this paper, we present flux distributions obtained on Bi-2212 single crystals in external magnetic fields up to 1 T. Until now, magneto-optical investigations of flux distributions were limited to low fields (≈ 300 mT) only [16–18]. The various defects found from the flux patterns are analyzed and it is shown that their effectivity as pinning sites can be studied in a very direct way.

2. Faraday effect and magneto-optical setup

We use the HRF technique to observe local flux structures with a relatively large spatial resolution (approximately of the order of the wavelength of the used light, i.e. ≈ 0.5 μm) [9,11].

This method is based on the Faraday effect in a thin magneto-optical layer deposited on a thin aluminium mirror film which is evaporated directly onto the sample [17]. The local flux is determined from the rotation of the polarization plane of linearly polarized light within the magneto-optical layer. In regions without flux, the light is reflected without rotation of the polarization plane. This light is thus not able to pass the analyzer which is set in crossed position with respect to the polarization plane of the incident light. In this way, the Meissner phase remains dark, whereas the Shubnikov phase is imaged bright. To achieve an optimal contrast, several conditions for the thickness of the magneto-optical active layer have to be fulfilled [4,17]. Clearly it is advantageous to use for the magneto-optical layer a compound with a large Faraday effect (high Verdet constant). For the work reported here we have used EuSe. The only disadvantage of EuSe is that it limits the temperature range to $T \leq 20$ K. This limit is imposed by the temperature-dependent Verdet constant leading to very low contrasts between the Meissner and the Shubnikov phase at higher temperatures [2,19]. The thickness of the EuSe layer is approximately 240 nm, the aluminium layer is 100 nm thick. In order to obtain the local magnetic field B_z, a calibration of the measured intensities is required. This can be carried out by comparison of the intensities of the sample with those of a SFL6 glass (showing a low Faraday effect itself) which is covered by the same magneto-optical layers [17,20].

For high resolution, a large numerical aperture of the optical system is required. Together with the mechanical constraints of the magnet this necessitates a short distance between the objective lens and the sample. Up to now this was realized by using a commercial polarization microscope for the observations, while a custom-built copper coil close to the objective generated the external field. Because of the space limitations of commercial microscopes the use of superconducting coils is not possible. As a consequence, magneto-optical observations were limited to low fields (max. 500 mT) [3,17]. In our microscope a large numerical aperture is realized by cooling the objective lens together with the sample [21]. For the present work, we used this custom built microscope which may be inserted into the variable temperature insert (1.5...300 K) of an Oxford Instruments cryostat equipped with either a 1 T or a 7 T superconducting coil. The sweep rate can be controlled between 0.05 mT/s and 40 mT/s. The sample is in helium exchange gas in order to have a good thermal equilibrium. A calibrated RhFe thermometer is mounted close to the sample to measure the sample temperature.

The images are recorded using a low-light level CCD camera system. The video signal is transferred to a video recorder equipped with a timecode signal (SONY EVO 3600P) for storage. During an experimental run, the timecode of the images plus other parameters such as the value of the external magnetic field and the temperature are recorded, so that the value of these parameters at every single image of the video tape is exactly known.

The Bi-2212 single crystals were grown by the travelling solvent floating zone method under an oxygen pressure of 200 kPa [22]. Small crystallites of approximately rectangular shape (typically $1.0 \times 1.0 \times 0.02$ mm^3) were cleaved from the bulk samples. The typical transition temperature of the crystals is around 90 K with a transition width $\Delta T_c \approx 1.5$ K.

3. Results and discussion

In all the magneto-optical images shown in this paper, the flux is imaged as bright areas whereas the

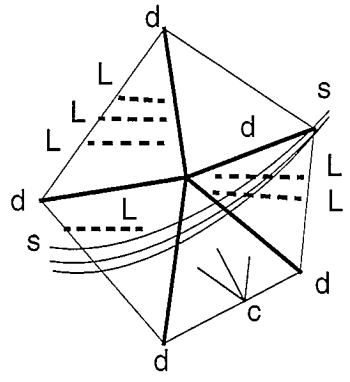

Fig. 1. Schematic representation of sample A. A group of surface step lines is indicated by the curved line labeled "ss". A crack in the surface is present at "c". A number of defect lines are labelled "L". The discontinuity lines of the currents are the five lines "d".

Meissner phase ($B = 0$) is dark. Unless otherwise noted, the temperature of observation is for all experiments $T = 2.5$ K.

First we discuss the penetration of flux into a Bi-2212 single crystal (sample A). The defect structure of this sample is shown schematically in Fig. 1. A group of surface step lines is indicated by the curved lines labeled "ss". A crack is present at "c". A number of defect lines are labeled "L". The so-called current-discontinuity lines induced by the five corners of the sample are the five lines "d". The penetration of flux into this Bi-2212 single crystal is shown on the left hand side of Fig. 2 starting from a zero-field cooled state [Fig. 2(a)]. The external magnetic field B_e is swept at a constant rate $dB_e/dt = 11.4$ mT/s to 0.2 T [Fig. 2(b)], 0.4 T [Fig. 2(c)], 0.6 T [Fig. 2(d)], 0.8 T [Fig. 2(e)], and up to 1 T [Fig. 2(f)]. At 1 T, the fully penetrated state is nearly reached even at this low observation temperature. The second row of images [Figs. 2(g–k)] are difference images between two subsequent fields. In this way it is clearly visible where flux has moved during the field sweep. The flux penetration starts in the lower right area of the crystal, where a small crack in the surface is present [marked by "c" in Fig. 1]. Such surface cracks are typical for Bi-2212 crystals and are shown to have a drastic influence on the flux patterns [23]. Upon raising the external magnetic field further, the *regular* flux penetration starting from the sample edges sets in. The depth of penetration is deeper near the center of each sample edge, whereas in the corners practically no penetration of flux takes place. This behavior is described in detail in Ref. [24]; briefly the reasoning is as follows: As the currents in the sample flow always parallel to the sample edges, in a polygon sample there must be a sharp bend of the currents. The lines where the currents are bending around are called discontinuity lines of the currents or d lines because along these lines the current density is reduced. These d lines (marked "d" in Fig. 1) end at the sample corners and are visible in the flux patterns up to relatively high applied external magnetic fields and can be washed away only by applying fields much larger than the full penetration field H^*. In our case there are five corners, so five d lines should be found. One of them is, however, severely disturbed by the influence of the surface crack already mentioned.

This expected pattern is further disturbed by a "finger-like" penetration along some optically invisible defects which we will analyze later on. Such a finger-like penetration of flux is well known from twinned $YBa_2Cu_3O_{7-\delta}$ single crystals [25–29]. However, at first sight the present behavior must have a different origin since twinning is not known for Bi-2212. At $B_e = 0.8$ T, a large number of these "fingers" is visible, even near the surface crack in the lower right area of the sample. Further increase of the external magnetic field leads to a more homogeneous pattern, while the effect of the fingers is still visible. The growth steps which are running as black lines through the sample center (running from "s" to "s" in Fig. 1) have no visible effect on the flux pattern thus demonstrating clearly that the magnetic distribution is a bulk effect.

The difference images [Figs. 2(g–k)] show *where* the flux has moved in the sample during the preceding field sweep. Between 0 T and 0.2 T, the flux penetrates the sample mainly along the surface crack where locally enhanced stray fields enable the flux to overcome the penetration barrier which is in the present case most probably a geometric barrier [30,31]. Along all other sample edges, only a small white rim of flux lines can be found. The next image [Fig. 2(h)], between 0.2 T and 0.4 T demonstrates that the penetration barrier has been overcome. Further increase of the external magnetic field leads to flux enhancement at the defects and all movement of

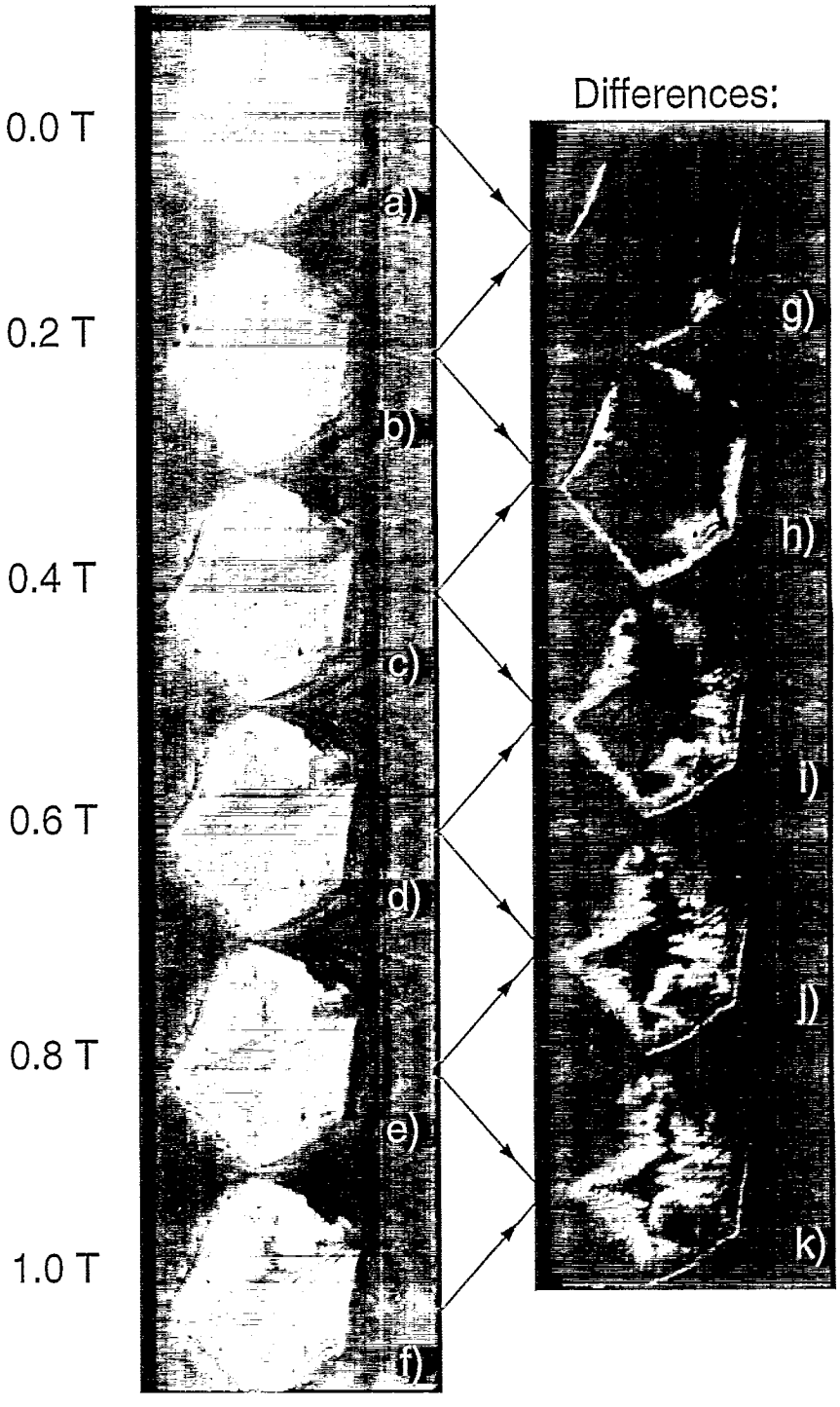

Fig. 2. Flux penetration into the Bi-2212 single crystal sample A in steps of 0.2 T up to the maximum field +1 T at a temperature $T = 2.5$ K. The flux is imaged as white areas, whereas the Meissner regions are black. The left column shows the flux penetration as real images, (a) −0 T, (b) −0.2 T, (c) −0.4 T, (d) −0.6 T, (e) −0.8 T and (f) −1.0 T. Differences between these images are shown in the right-hand column as follows: (g) is (b) minus (a), (h) is (c) minus (b) etc. The external magnetic field is swept at a rate $dH_e/dt = 11.4$ mT/s. The influence of the surface crack (c in Fig. 1) is clearly visible. Also, some "flux fingers" ("L" in Fig. 1) form which show similar behavior as in twinned $YBa_2Cu_3O_{7-\delta}$. The subtracted images show where the flux has *changed*. In (g), only a small penetration of flux takes place, confined to the sample edges and to the surface crack. Between 0.2 T and 0.4 T (h), the flux entrance barrier breaks down and we find a large flux penetration. The left half of the crystal shows already the typical geometry-dependent shape (see text). The next images, (i), (j) and (k) demonstrate how the flux rushes deeper into the sample. There is, however, no change at the sample edges; the flux moves mostly along the various defects and into the Meissner area in the center.

flux takes place only in the direction towards the field-free Meissner area.

On most Bi-2212 single crystals a Bean-like model for the critical state [32] cannot be applied due to the irregular flux penetration caused by the surface cracks. If the defects are widely spread over the sample, the zones of flux may even merge with each other and form separated areas. This leads to a kind of field-induced granularity as the Meissner currents (shielding currents) are flowing now on a smaller length scale in the crystallites between the defects [33]. Instead of one current loop shielding the whole sample, there are then several loops, each shielding only a small part. At constant *current* the magnetic field of a planar current loop is unchanged if the loop is replaced by several sub-loops spanning the

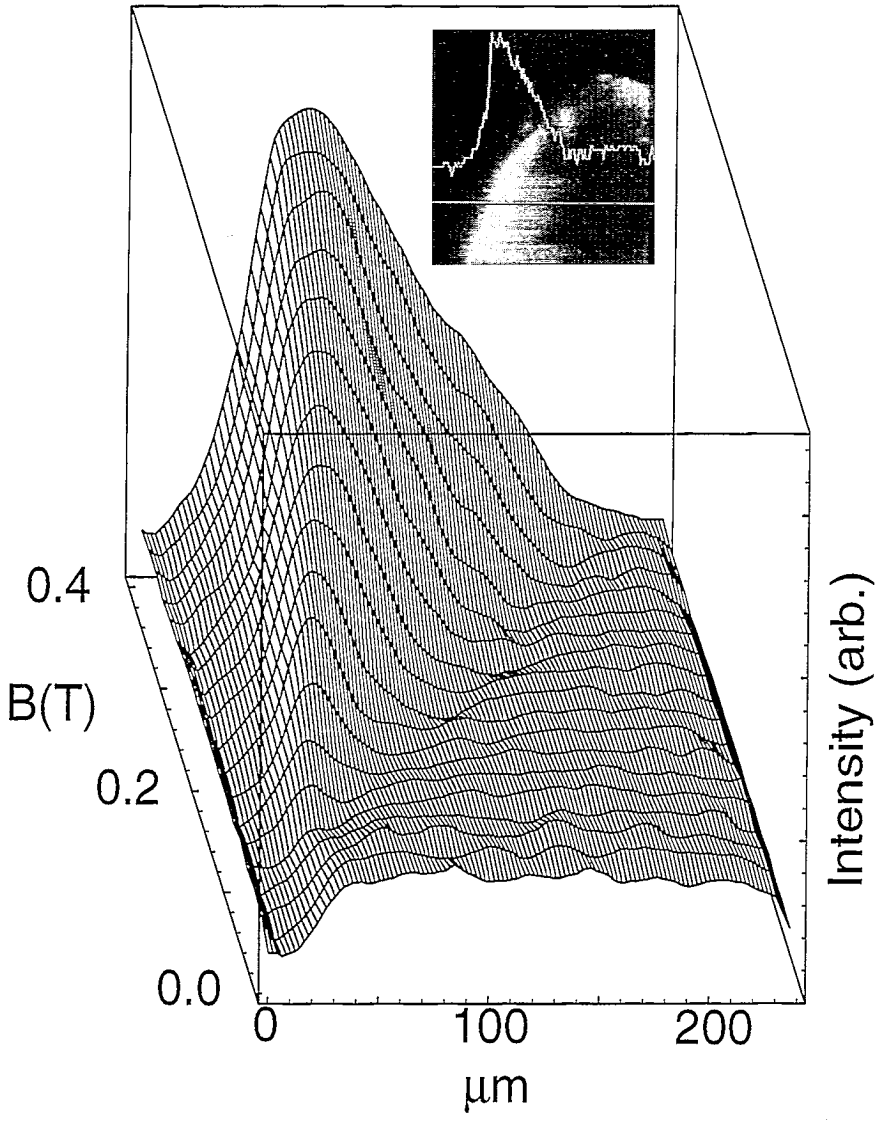

Fig. 3. 3D plot for sample A of the smoothed flux-density profiles (given here as measured intensity in arbitrary units) in the field range 0–0.4 T. The sample edge is located at 0 μm. Outside the sample the magnetic field is not shown (see text). The area where the profiles are read is illustrated in the insert, which shows the upper left hand corner of the crystal. Also shown is a "raw" profile.

same area. This can be nicely demonstrated using magneto-optical observations of samples with a well-defined grain boundary, e.g. using bicrystals or thin films covering bicrystalline substrates or substrates with surface steps [34]. However, at constant *current density* the field decreases when the number of sub-loops increases. Hence, even if the critical current density is unaffected by the defects, the magnetic moment of samples with defects leading to current sub-loops will be significantly reduced. Conversely one will severely underestimate the critical current density of such a sample if the critical current is determined from its magnetic moment (with the tacit assumption of a single current loop shielding the whole sample). The magneto-optical observation of defect-modified flux penetration can be used to calculate the necessary corrections. Below (with sample B) we will encounter an even clearer example of disturbed shielding currents.

In Fig. 3, smoothened flux density profiles are shown as a function of the external magnetic field in a three-dimensional plot corresponding to the images of Fig. 2 for magnetic fields between 0 and 0.4 T. The local flux density is represented uncalibrated as measured intensity in arbitrary units. The position on the sample where the flux-density profiles are read is shown in the insert as the white line. The corresponding "raw" flux-density profile is represented separately. The sample edge is on the left side of the plot at 0 μm. The magnetic field outside the sample is not shown since for this sample, the magneto-optical film was covering the sample only. Along lines which are parallel to the defect lines "L", the flux-density profiles are homogeneous and very much like that of a defect-free sample. This shows that the flux gradient next to and along the defect lines is practically undisturbed.

The remanent state, which is formed after sweeping the external magnetic field to 1 T and then back to 0 T, is presented in Fig. 4. The pinned flux now

Fig. 4. The remanent state of sample A, obtained after sweeping the external magnetic field to +1 T and back to 0, using a sweeprate $dH_e/dt = 11.4$ mT/s. The pinned flux stays in the center of the sample, and along the edges vortices of opposite polarity appear. The areas with reduced vortex density are due to annihilation effects (see text). As the sample has five corners, the shape of the pinned flux domain has peaks which point to each of these corners as predicted by the d line concept ("d" in Fig. 1, see also text).

remains where movement is reduced i.e. at the d lines [23,25,35]. Due to the curvature of the flux lines in these thin samples, the field lines of the trapped flux close around the sample and thus induce negative flux in the sample edges, also clearly visible in Fig. 4. The sign of the vortices can be directly found by turning the polarizer as described in Ref. [35]. Between the pinned flux lines and the negative vortices there is a wide area where the flux density is strongly reduced. This is caused by annihilation of vortices and anti-vortices.

To study the influence of the defects on the pinning behavior, "conventional" flux-creep experiments are performed on the same crystal, e.g. the external magnetic field is swept first to 1 T, then back to 0 T and kept constant. The time dependence of the flux distribution is then recorded. Fig. 5 shows a difference image between the first image taken at $t = 0$ s and the image taken at $t = 625$ s. In this representation it is clearly visible in which areas of the sample the flux relaxes. Large areas of flux along the sample edges are found to stay constant in time. The vortices move mainly along the flux-density gradients into the existing Meissner area. Also along the flux fingers there is a large time-dependent penetration. This relaxation experiment demonstrates clearly that the presence of defects in the sample opens more ways for the flux lines to relax.

To investigate the nature of the defects found magneto-optically, some X-ray experiments were performed. However, since the sample A shown in Figs. 1–4 was very small and covered with an aluminium and EuSe layer, the diffraction spectra were unsatisfactory. Therefore we decided to continue our investigations on a larger crystal B from the same batch. In Fig. 6(a) we show an image of this second crystal taken with an ordinary microscope. This crystal was not covered by magneto-optical layers. Instead we used an SFL-6 glass substrate covered with the magneto-optical layers in close

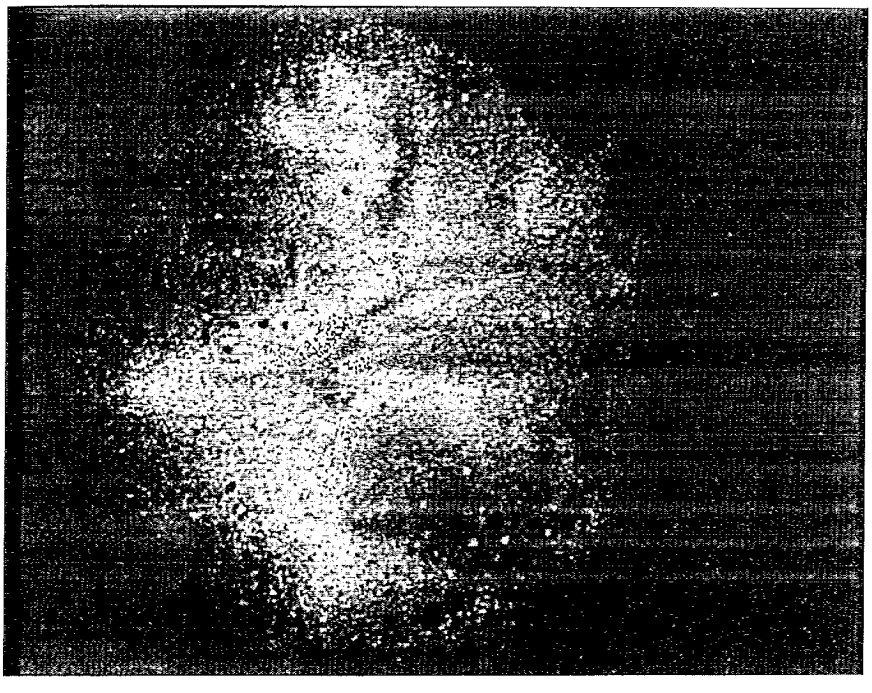

Fig. 5. Image of the relaxation areas in sample A, obtained from the relaxation of the state of Fig. 4 and shown as a difference image between the images taken at the end point of the relaxation, $t = 625$ s and at the start at $t = 0$ s. The areas to which flux has moved are represented in white. Most of the relaxation has taken place at the "flux fingers"; less relaxation is found in the defect-free areas. The areas along the sample edges have a much smaller contribution to the relaxation.

contact with the sample to observe the flux pattern. In Fig. 6(b) we show the magneto-optical image at 0 T, after the field was swept to 1 T and back to zero again. Clearly there is a long horizontal line (parallel to the longest axis of the sample) which is very similar to the defect lines in sample A. Also other defect lines are clearly visibly which divide the sample in eight "islands". The screening currents of the sample appear to be confined within the islands. Hence the total magnetic moment is about one order of magnitude lower than for the same sample without defects. Conversely, if the critical current of this sample would be calculated from its total magnetization under the assumption that there were no defects, one would find a critical current which is about one order of magnitude lower that the real shielding currents of the "islands".

It is interesting to note that only a few of these islands can be related directly to the defects visible in the photograph of the sample Fig. 6(a). The reason

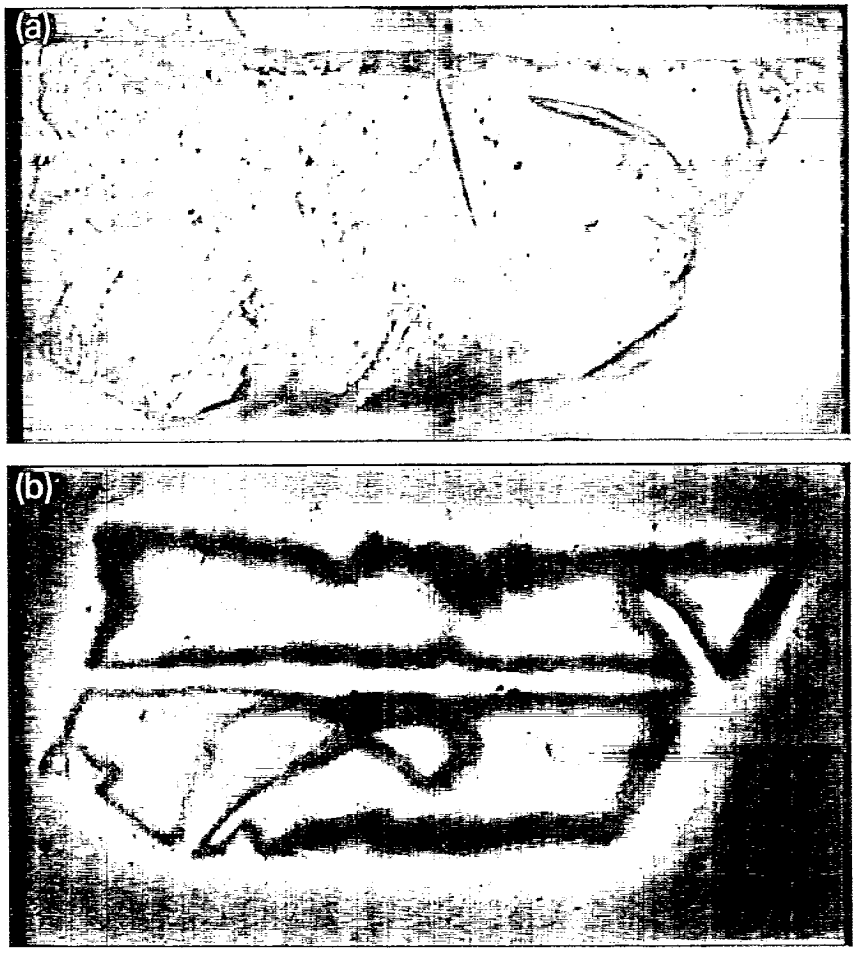

Fig. 6. (a) Image of sample B, another Bi-2212 single crystal of the same batch, obtained using ordinary microscopy. Some surface cracks are visible. (b) Magneto-optical image of the same crystal. The external magnetic field is 0 T after the field had been previously swept to 1 T and back to zero again; the temperature is $T = 2$ K. Clearly visible is a very long line running parallel to the largest edge of the crystal. It is important to note that this magneto-optically observed line cannot be correlated directly to the defects visible in (a). This sample was also used for the X-ray studies.

for the very large horizontal defect running along the whole length of the sample is not visible in this photograph. This demonstrates clearly that the magnetic patterns show defects in crystals which cannot be seen with ordinary optical detection techniques.

X-ray measurements on this second sample yield very good spectra. There is no evidence for other phases than Bi-2212 (see Fig. 7), except for a very small peak at approximately 40°. However, the rocking curve for rocking along the long magneto-optically visible defect line [Fig. 8 (a)] is much wider than for rocking along a line perpendicular to it as shown in Fig. 8(b). Although we have no direct evidence, our measurements are consistent with the following picture. This Bi-2212 "single" crystal is in fact composed of a few crystallites. These are separated by straight defect lines which in general run along the whole length of the crystal and parallel to one of the edges. Two adjacent crystals have a c-axis which is pointing in a slightly different direction in the plane which is perpendicular to the defect line. This situation is schematically drawn in Fig. 9. Along the boundaries are weak superconducting links, where vortices can rush along and form the flux fingers as found in the magneto-optical observations. The structure of such grain boundaries in other

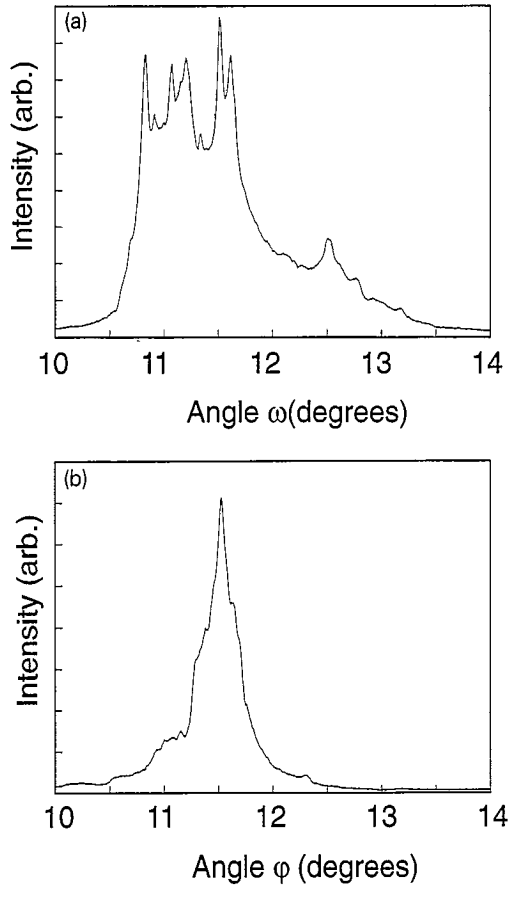

Fig. 8. Rocking curves of the peak at $2\Theta = 23°$ for sample B measured in two different directions; (a) for rocking along an axis in the twin plane: ω (see Fig. 9) is varied. Due to the various directions of the c-axis a very broad rocking curve is observed. The non-gaussian rocking curve is not unusual for $Bi_2Sr_2CaCu_2O_{8+\delta}$; (b) for rocking along an axis perpendicular to the "twin plane": ϕ (see Fig. 9) is varied.

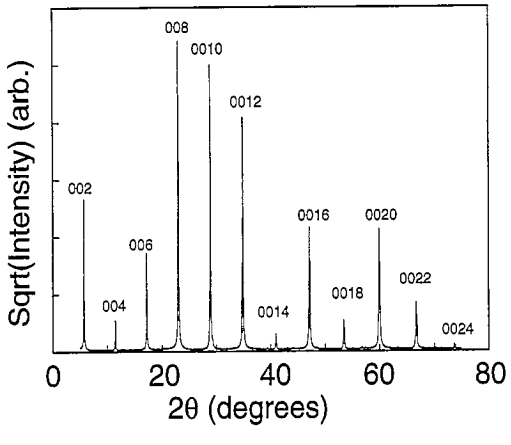

Fig. 7. X-ray diffractogram of sample B (Θ–2Θ scan in the Bragg–Brentano geometry). No evidence for other phases than Bi-2212 is found, except for a very small peak at approximately 40°. The splitting of the 0016 and higher reflections is due to the presence of both the Cu $K\alpha_1$ and $K\alpha_2$ lines in the X-ray source.

samples was previously analyzed using TEM microscopy [36]. Along the boundary other chemical phases were found. Due to the small width of the boundary these do not show up in our X-ray measurements except for the small peak at approximately 40°. Known defects within the Bi-2212 crystals are intergrowths of Bi-2223 phase [37], which show up in resistivity measurements. On a larger crystal of the same batch as the crystals under study we have seen two transitions, e.g. one at 110 K and a second but larger one at 90 K. Another known type of

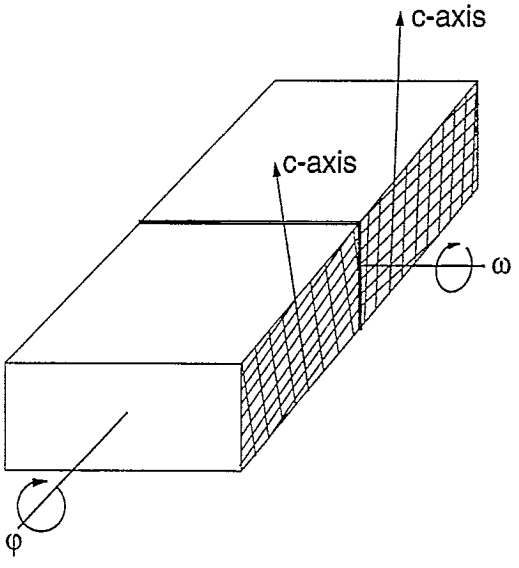

Fig. 9. Schematical representation of the defects causing the finger-like penetration pattern seen in the magneto-optical images. The thick horizontal line separating the front and back halves of the crystal corresponds to the horizontal defect line in Fig. 6(b). The spread of the c-axis orientation is about 1 degree along the ω direction, while it is only 0.4 degrees along the ϕ direction.

intergrowth consists of remnants of the solvent from which the crystals are grown.

4. Conclusions

In this paper we have presented flux distributions of two typical Bi-2212 single crystals up to an external magnetic field of 1 T. For the first time we have analyzed the flux–defect interaction in $Bi_2Sr_2CaCu_2O_8$ single crystals in detail. A finger-like penetration of flux similar to the penetration of flux lines along twin boundaries in $YBa_2Cu_3O_{7-\delta}$ single crystals was observed. This behavior is possibly caused by a misorientation of the c-axis; e.g. the crystal is composed of a few crystallites with c-axes which deviate about one degree from each other. We also observed that growth steps do not show a significant influence on the flux distribution. Defects along which the flux penetrates very quickly separate the sample magnetically into smaller parts. As a consequence these defects are found to have a crucial influence on the magnetization behavior of the sample. Even if the critical currents are unaffected by the defects, the magnetization of samples with defects leading to current sub-loops will be significantly reduced. The magneto-optical observation of defect-modified flux penetration can be used to calculate the necessary corrections.

Acknowledgements

We thank R. Bakker for help with some of the measurements. This work is part of the research program of the Stichting voor Fundamenteel Onderzoek der Materie (FOM), which is financially supported by NWO.

References

[1] M.R. Koblischka and R.J. Wijngaarden, Supercond. Sci. Technol. 8 (1995) 199, review article.
[2] R.P. Huebener, Magnetic Flux Structures in Superconductors, Solid State Sciences 6 (Springer, New York, 1979), and references therein.
[3] N. Moser, M.R. Koblischka, B. Gegenheimer, H. Kronmüller and H. Theuss, Physica C 159 (1989) 117.
[4] M.R. Koblischka, N. Moser, B. Gegenheimer and H. Kronmüller, Physica C 166 (1990) 36.
[5] H. Theuss, A. Forkl and H. Kronmüller, Physica C 190 (1992) 345.
[6] M.V. Indenbom, N.N. Koleshnikov, M.P. Kulakov, I.G. Naumenko, V.I. Nikitenko, A.A. Polyanskii, N.F. Vershinin and V.K. Vlasko-Vlasov, Physica C 166 (1990) 486.
[7] D. Kirchgässner, P. Brüll and P. Leiderer, Physica C 195 (1992) 157.
[8] H. Kirchner, Phys. Lett. A 30 (1969) 437;
idem, Phys. Status Solidi 4 A(1971) 531.
[9] M.R. Koblischka, Th. Schuster, B. Ludescher and H. Kronmüller, Physica C 190 (1992) 557.
[10] R.J. Wijngaarden, M.R. Koblischka, R. Griessen and A.A. Menovsky, to be published.
[11] M.R. Koblischka, thesis, University of Stuttgart, (1992).
[12] A. Forkl, H.U. Habermeier, R. Knorpp, H. Theuss and H. Kronmüller, Physica C 211 (1993) 121.
[13] M. Leghissa, Th. Schuster, W. Gerhäuser, S. Klaumünzer, M.R. Koblischka, H. Kronmüller, H. Kuhn, H.W. Neumüller and G. Saemann-Ischenko, Europhys. Lett. 11 (1993) 323;
Th. Schuster, M.R. Koblischka, H. Kuhn, H. Kronmüller, M. Leghissa, W. Gerhäuser, G. Saemann-Ischenko, H.W. Neumüller and S. Klaumünzer, Phys. Rev. B 46 (1992) 8496.
[14] J.C. Martinez, S.H. Brongersma, D.G. de Groot, R. Griessen, B. Ivlev and P.H. Kes, Phys. Rev. Lett. 69 (1992) 2276.

[15] M.V. Indenbom, A. Forkl, B. Ludescher, H. Kronmüller, H.U. Habermeier, B. Leibold, G. D'Anna, T.W. Li, P.H. Kes and A.A. Menovsky, Physica C 226 (1994) 325.
[16] B. Ludescher, Th. Schuster, M.R. Koblischka, N. Moser and H. Kronmüller, Laser Optoelektron. 23 (1991) 54.
[17] Th. Schuster, M.R. Koblischka, N. Moser, B. Ludescher and H. Kronmüller, Cryogenics 30 (1991) 811.
[18] K.-H. Greubel, E. Gmelin, N. Moser, Ch. Mensing and L. Walz, Cryogenics 30 (suppl.) (1990) 457.
[19] J. Schoenes, Z. Phys. B 20 (1975) 345;
G. Busch and P. Wachter, Z. Angew. Phys. 26 (1969) 1.
[20] A. Forkl, H.U. Habermeier, B. Leibold, T. Dragon and H. Kronmüller, Physica C 180 (1991) 155.
[21] R.J. Wijngaarden, M.R. Koblischka and R. Griessen, Physica C 235–240 (1994) 2699.
[22] T.W. Li, P.H. Kes, H.T. Hien, J.J.M. Franse and A.A. Menovsky, J. Cryst. Growth 135 (1994) 481.
[23] Th. Schuster, M.R. Koblischka, N. Moser and H. Kronmüller, Physica C 179 (1991) 269.
[24] Th. Schuster, M.V. Indenbom, M.R. Koblischka, H. Kuhn and H. Kronmüller, Phys. Rev. B 49 (1994) 3443.
[25] Th. Schuster, M.R. Koblischka, B. Ludescher and H. Kronmüller, J. Appl. Phys. 72 (1992) 1478; idem, Z. Metallk. 83 (1992) 618.
[26] L.A. Dorosinskii, M.V. Indenbom, V.I. Nikitenko, A.A. Polyanskii, R.L. Prozorov and V.K. Vlasko-Vlasov, Physica C 206 (1993) 360.
[27] M. Turchinskaya, D.L. Kaiser, F.W. Gayle, A.J. Shapiro, A. Roytburd, V.K. Vlasko-Vlasov, A.A. Polyanskii and V.I. Nikitenko, Physica C 216 (1993) 205.
[28] L.A. Dorosinskii, V.I. Nikitenko, A.A. Polyanskii and V.K. Vlasko-Vlasov, Physica C 219 (1994) 81.
[29] U. Welp, T. Gardiner, D. Gunter, J. Fendrich, G.W. Crabtree, V.K. Vlasko-Vlasov and V.I. Nikitenko, Physica C 235–240 (1994) 241.
[30] Th. Schuster, H. Kuhn, E.H. Brandt, M.V. Indenbom, M.R. Koblischka and M. Konczykowski, Phys. Rev. B 50 (1994) 16684.
[31] B. Khaykovich, E. Zeldov, M. Konczykowski, D. Majer, A.I. Larkin and J.R. Clem, Physica C 235–240 (1994) 2757;
E. Zeldov, A.I. Larkin, V.B. Geshkenbein, M. Konczykowski, D. Majer, B. Khaykovich, V.M. Vinokur and H. Shtrikman, Phys. Rev. Lett. 73 (1994) 1428.
[32] C.P. Bean, Rev. Mod. Phys. 36 (1964) 31;
H.P. Wiesinger, F.M. Sauerzopf and H.W. Weber, Physica C 203 (1992) 121.
[33] M.R. Koblischka, Th. Schuster, H. Kuhn and G. Ravi Kumar, to be published.
[34] Th. Schuster, M.R. Koblischka, H. Kuhn, H. Kronmüller, G. Friedl, B. Roas and L. Schultz, Appl. Phys. Lett. 62 (1993) 768.
[35] Th. Schuster, M.R. Koblischka, H. Kuhn, M. Leghissa, M. Kraus and H. Kronmüller, Physica C 196 (1992) 429.
[36] O. Eibl, Physica C 168 (1990) 231.
[37] H.W. Zandbergen, private communication.